Journal of Palaeogeography

ORIGINAL ARTICLE Open Access

Ancient rip current records and their implications: an example from the Cretaceous Ukra Member, Kutch, India

Subir Sarkar* and Amlan Koner

Abstract

Poorly-sorted conglomerate patches rich in granules or sturdy fossils or both, and reddish mud matrix within the interstices stand out amidst fine-grained siliciclastic shelf sediments of the trangressive systems tract (TST) of the Lower Cretaceous Ukra Member, Kutch Basin, India. The siliciclastic shelf sediments contrast the conglomerates with their remarkable lateral extension. The fossils belong to a low-diversity group of sedentary bivalves that can be traced into the shoreface facies assemblage. The shelf sandstones are almost always sculpted by wave structures, especially hummocky cross-stratification while textures in the conglomerates suggest that the sediment settling was generally from suspensions. Textural variations in conglomerates reflect an immediate variation in flow viscosity prior to the downloading. The current structures obtained from the conglomerates record offshoreward palaeocurrent, in contrast to the shore-parallel palaeocurrent in the TST. The hummocky cross-stratified (HCS) beds are interpreted as seasonal storm deposits, while the conglomerate patches are taken as rip current deposits induced by waves of much longer periods. The glauconite-rich shale that alternates with conglomerates is probable fair-weather products. The conglomerates could not be recognized either in the coarse-grained shoreface deposits occupying the lower part of the overall fining-upward TST or in the coarsening-upward and glauconite-depleted highstand systems tract (HST). In contrast to the TST, the HST is dominantly tide-imprinted, having shore-normal palaeocurrent direction. It appears that intensification of waves and weakening of tides during transgression favored strong rip currents generation, which had presumably caused severe damage to the sea coast and to the shell banks growing preferably at the necks of the rip current channels. Rapid lateral facies transitions in the shoreface deposits at the basal part of the TST suggest enhanced irregularity in the coastline, possibly because of the mega cusps indented upon it. Frequency and intensity of storms enhanced during periods of global warming caused the transgression of the Early Cretaceous Ukra Sea.

Keywords: Rip current fan, Ukra Member, TST shelf, Longshore current, Shore-normal flux, Mass flow deposits, Global warming, Ukra Sea

1 Introduction

Rip current is named by Shepard (1936) and is present in almost all the seashores around the globe. Wind-stress pushes waves shoreward, and the water thus piled up moves alongshore till across-shore low stress allows it to return to the sea (Inman and Brush 1973; Smith and Largier 1995; Grant et al. 2005; Clarke et al. 2007; Reniers et al. 2009; MacMahan et al. 2010; Marchesiello et al. 2015). In this process momentum of the incoming wave transforms into a group of waves of variable height that interact amongst themselves and also with the alongshore currents, and both the waves as well as the currents interact with the shoreline topography to generate the offshore-directed rip current (MacMahan et al. 2006; Dalrymple et al. 2011). Rip current is the most

* Correspondence: jugeoss@gmail.com
Department of Geological Sciences, Jadavpur University, Kolkata 700 032, India

efficient mechanism for mass transfer of materials from shore to offshore (Shepard et al. 1941; McKenzie 1958; Short 1985; Smith and Largier 1995; Marchesiello et al. 2015). Rip velocities up to 1 m/s have been measured on the sea surface by Short and Hogan (1994). The low incidence, low tide and undulations of the rip current, however, become stronger with strengthening of the incoming wave, in the shore-line topography. Storms thus make rip currents formidable; typhoons and tsunamis drive them fastest; and, the breaker zone is penetrated through by them and the shore-zone materials may get transported on to the shelf (MacMahan et al. 2010; Yang et al. 2017).

A large body of literature has been generated on rip currents primarily because the currents threaten life of the swimmers (Macmahan et al. 2006, 2010 and references therein). Since the days of Shepard and Inman (1950), numerous field studies, laboratory simulations and numerical models in both 2D and 3D formats have enhanced our understanding about the genesis and flow patterns of rip currents (Shepard and Inman 1950; Arthur 1962; Longuet-Higgins and Stewart 1962; Tam 1973; Noda 1974; Davidson-Arnott and Greenwood 1974, 1976; Birkemeier and Dalrymple 1975; Sasaki and Horikawa 1975, 1978; Clifton 1976; Komar 1976; Greenwood and Davidson-Arnott 1979; Lenhart 1979; Greenwood and Hale 1980; Thompson 1981; Wright 1982; Basco 1983; Short 1985; Wu and Liu 1985; Bowman et al. 1988a, 1988b).

Rip current deposits are, however, seldom addressed in literature possibly because of the difficulty in collecting details about them under the sea and the uncertainty of their distinctiveness in case of their ancient counterparts. Nonetheless, rip current deposits are expected to stand out amidst finer-grained association and hence should have higher preservation potential. Products of the stronger rip currents induced by longer period waves are likely to have more remarkable differences from sediments of other origins. Some probable examples of ancient rip current deposits were recognized on the basis of their common channelized forms; the grain size of these recognized deposits, which were usually enriched in sturdy fossils (mostly of sedentary organisms), was discretely coarser than the background sediments (Kazmierczak and Goldring 1978; Lewis 1980; Clifton 1981; Hart and Plint 2003; Ślączka et al. 2011). The rip current deposits were visualized by Lewis (1980) as small fan-like bodies; he reported convex-up bodies and considered rip current deposits as debris flow products (see also Ślączka et al. 2011). Wide variability in forms and textures of the rip current deposits was described by Gruszczyński et al. (1993), and, MacMahan et al. (2006) further refined the relevant observations and put them in the background of flow dynamics. Picard and High (1968) depended on the ripple orientation at high angle to the palaeoshoreline to recognize rip current deposits in a Triassic formation.

The present paper addresses multiple potential rip fan deposits in the Ukra Member of the Lower Cretaceous Bhuj Formation in Kutch Basin, western India (Fig. 1). A unified model of the rip fan sedimentation has also been proposed to inspire more intense searches for ancient rip current deposits to generate a clearer idea about the frequency of past occurrence of excessively strong storms. Importance of such an endeavor lies in the fact that ancient rip current deposits can be conceived as good palaeoclimatic indicators and as a corollary, they should also have considerable stratigraphic significance. Aimed at the latter one, we studied the general character and evolution of the entire Ukra Member, although the deposits of the specific concern were recognized only in its middle tier.

2 Geological setting

The 77 m-thick marine siliciclastic deposits of the Lower Cretaceous Ukra Member accumulated in the Mesozoic Kutch Basin, India in the late stage of syn-rifting phase (Biswas 2016a). The Ukra Member is confined to the west of the NNE-SSW oriented Median Ridge that divided the Kutch Basin into two (Biswas 1987, 2016b). Succeeding the lagoonal Ghuneri Member upward (Bose et al. 1986), the Ukra Member of open shelf origin attests to marine transgression (Rajnath 1932; Spath 1933; Biswas 1977; Fürsich and Pandey 2003; Bansal et al. 2017). The palaeoshoreline trended NNW-SSE (Biswas 1991). The Bhuj Formation is generally devoid of mega fossils; the only exception is the Ukra Member that has sporadic occurrences of nektonic ammonites and pockets of benthic trigonia (Spath 1933; Krishna 1987; Fürsich and Pandey 2003; Rudra and Bardhan 2006). Fürsich and Pandey (2003) recognized *Seebachia*, *Herzogina*, *Gryphaea*, *Gervillella*, *Megacucullaea*, *Pisotrigonia* and *Indotrigonia* within the fossil population. The aforementioned transgression has been attributed to the global event of sea level rise at the interval between the Albian and the Aptian (Biswas 2016b). The Median Ridge dividing the Kutch Basin was drowned during the course of this sea level rise. The inland marine deposit on the east of Median Ridge that equates with the Ukra Member on the west has been comprehensively studied by Mandal et al. (2016). The sedimentological account of the younger two tiers of the 3-tiered Ukra Member with a focus on glauconite distribution has recently been addressed by Bansal et al. (2017). The Ukra Member rests on a transgressive lag (Fig. 2a) and is overlain by the Upper Terrestrial Member (Mandal et al. 2016). Bansal et al.

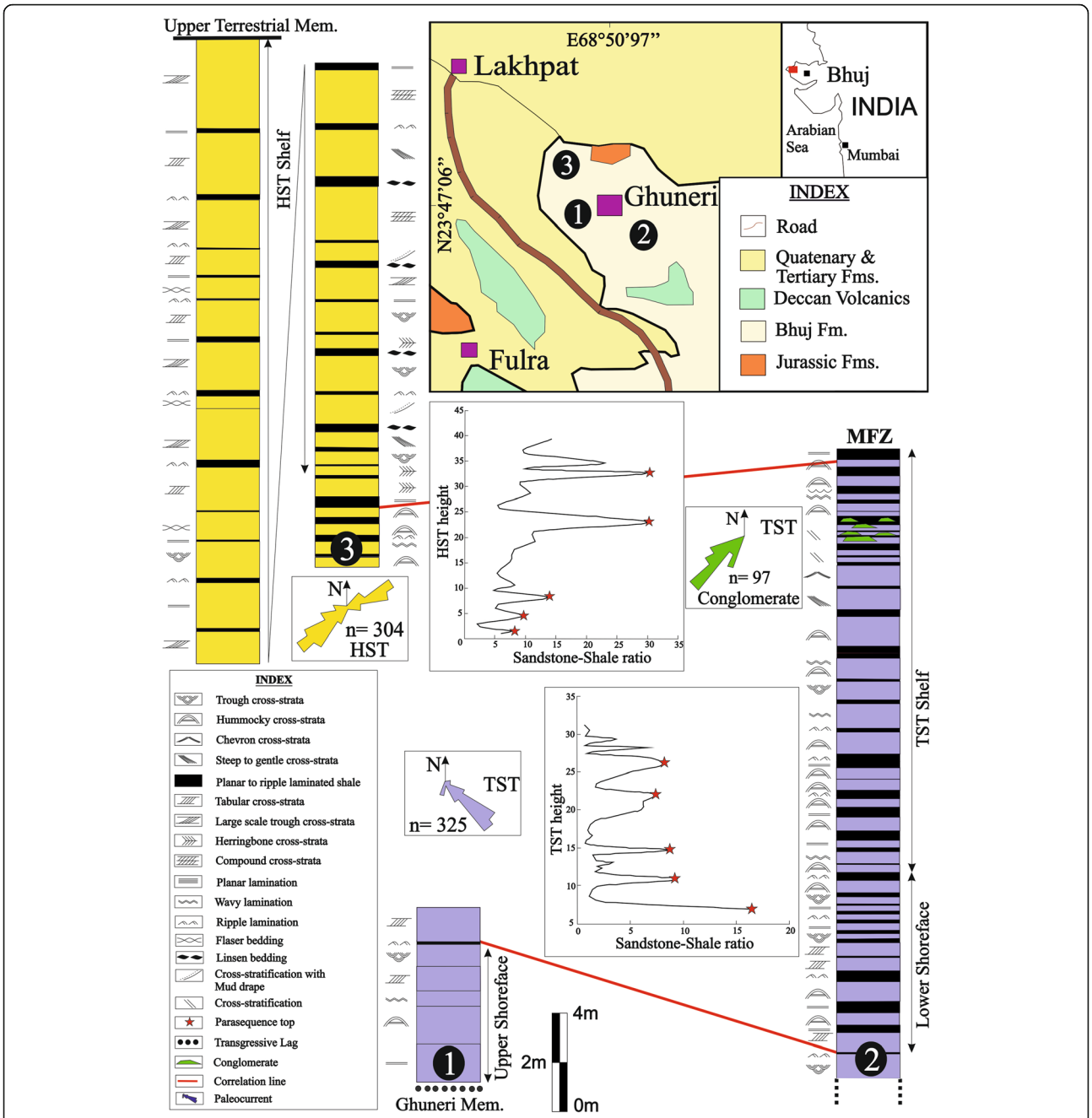

Fig. 1 Geological map on top right, within a portion of the map of western India. The numbered dots in the location map indicate the positions of the measured sections. Within the inset map, the red rectangle marks the study area in regional context. All sections represent the Ukra Member, divided into shoreface, TST shelf and HST shelf facies assemblages, with their variations in lithology and sedimentary structure. Sandstone–shale ratio and delineated parasequences within the TST and the HST are depicted in the associated curves. Palaeocurrent directions of the shoreface, the TST shelf and the HST shelf are given in roses separately. Fm. = Formation; Fms. = Formations; Mem. = Member; MFZ = Maximum flooding zone

(2017) aptly recognized the middle tier as a TST and the top tier as a HST. Glauconite content overall increases up the TST and reaches the highest content in the maximum flooding zone (MFZ). Above the MFZ, the upward coarsening HST is depleted in glauconite. However, the basal tier of the Ukra Member, seemingly of shoreface origin, remained excluded from the account of Bansal et al. (2017).

3 Methodology

This field-based study depended upon thorough and crucial field observations using commonly deployed

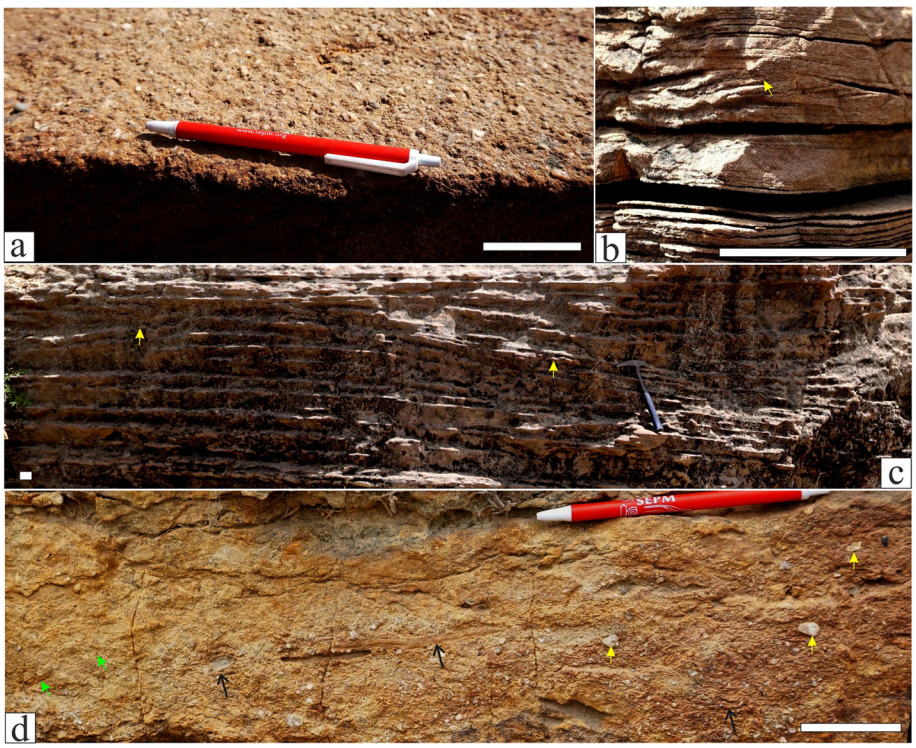

Fig. 2 A upper shoreface facies assemblage: **a** Transgressive lag between the Ghuneri Member and the overlying Ukra Member; **b** Planar laminated facies locally encasing isolated ripple forms (arrow); **c** Hummocky cross-stratification (arrows) in coarse-grained sediment; **d** Large scale cross-stratified facies within granule- and fossil-rich (arrows) facies. Scale bar = 5 cm

field equipment, like clinometer, measuring tape, pocket lens, pocket knife, hammer, GPS and camera. Observations were made bed by bed, parasequence by parasequence. Sediment grain-size variations and the variation in grain sorting were estimated with the help of pocket lens. Palaeocurrent data were collected using mainly the cross-strata orientations from different stratigraphic segments separately. Cross-strata and clinoform orientations were used to reveal the transport direction of the purported rip currents. The ratio of sandstone to shale was determined from successive couplets, each constituted by a sandstone package and a shale package that overlies it. Rip current deposits are identified and their depositional mechanism is based mainly on the huge literature available on their counterparts in the modern world.

4 Results

4.1 General sedimentology of the three tiers of the Ukra Member

Maintaining continuity with the previous sedimentological findings of Bansal et al. (2017), we present facies types of the Ukra Member under three facies assemblages named interpretatively as shoreface, shelf 1 (TST shelf), and shelf 2 (HST shelf), from bottom upward (Fig. 1). However, these facies assemblages are analyzed and interpreted mainly based on their depositional and palaeogeographic features respectively on the basis of their intrinsic details and associations. Since Bansal et al. (2017) with their specific focus on the glauconite occurrence laid emphasis on the shelf, the facies constituents of each of the assemblages are thus dealt with here, from base upward, rather cryptically as follows.

4.2 Shoreface assemblage

This sandstone-rich facies assemblage is 18 m-thick, showing a fining upward trend, and incorporates reddish mudstone beds in the top. The assemblage is subdivided into two: the lower subdivision (TU) and the upper subdivision (TL). The lower subdivision (TU) extends upward till a mudstone bed turns up. Thicknesses of the two subdivisions are discernibly variable in different localities.

A planar-laminated, fine-grained and well-sorted sandstone facies (TUa) overlies the transgressive lag directly. Locally these laminae encase isolated asymmetric ripples draped by sandstone facies without any discernible change in grain-size composition (Fig. 2b). At certain instances, the ripple laminae imperceptibly pass laterally into planar laminae. The isolated ripples have height around 2.7 cm and spacing of 8.5 cm. At

places, in the field outcrop, the laminae are broadly wavy in fine and well-sorted sand grade sediment. Broad channels are locally incised into the similar planar or wavy laminae of the channel facies TUb. The channel-filling laminae often tend to mimic the configuration of the channel-base, but discernibly thicken at the deepest part. Some channel-fills are distinctly coarse and bear mud clasts as well as granule-sized quartz grains. Subcritically climbing ripples fill in such channels. A wavy-laminated, fine-grained and well-sorted sandstone facies (TUc) overlies the dominantly planar-laminated facies TUa and the channel facies TUb. Laterally as well as vertically, the preceding facies give way to the coarse-grained and moderately-sorted sandstone facies that is characterized by the large-scale hummocky cross-stratification (TUd; Fig. 2c). This facies TUd also directly overlies the transgressive lag locally. Poor quality of exposure prevents exact measurements of the dimensions of these HCS beds; however, their estimated wave length exceeds a meter by far. The facies TUd is succeeded upwards by a wavy-laminated fine-grained sandstone facies TUe which, in turn, almost imperceptibly gives way upward to a coarse-grained, even granular, trough cross-stratified sandstone facies TUf. The facies TUf attains 55 cm in preserved thickness, and within it, the trough cross-stratified sandstone is measured 9 cm in thickness on average. The facies TUf sparsely contains granular quartz grains and large bivalve shells (Fig. 2d). Besides, there is a tabular cross-stratified sandstone facies TUg, the thickness of which is measured around 1.6 m. Although there is locally a clear indication of bedform climb, in which the thickness of the tabular cross-stratified sandstone shortens, in a range of around 20 cm.

In the TL subdivision, the mudstone facies TLa (Fig. 3a) is generally reddish in color, intensely bioturbated, and has vertically variable thickness with an overall tendency of upward thickening. The maximum thickness of this facies reaches 45 cm. At the field outcrop, this facies almost imperceptibly grades into a fine-grained tabular cross-stratified sandstone facies TLb (Fig. 3b). The preserved thickness of the tabular cross-stratified sandstone ranges up to 63 cm. With the transition from mudstone to sandstone, the burrowing intensity decreases abruptly. Burrows are either dominantly vertical and filled with the sandstone bodies, or dominantly horizontal to oblique and filled with the mudstones. The mudstone-filled burrows in the facies TLa are grayish in contrast to the reddish background of the facies. A hummocky cross-stratified and fine-grained sandstone facies TLc develops with tabular geometry, and the wave length of its large HCS beds is longer than 2 m. The minimum thickness of this facies is about 35 cm. The palaeocurrent attributed in the entire shoreface assemblage is parallelly-oriented to the palaeshoreline mentioned above (Fig. 1).

4.2.1 Interpretation

The planar-laminated facies TUa is likely the product of sheet-flow, and on top of the transgressive lag, it appears

Fig. 3 A lower shoreface facies assemblage: **a** Intensely bioturbated mudstone facies. Note mud-filled burrows (marked by yellow arrows) occurring frequently; **b** Fine-grained tabular cross-stratified sandstone facies. Scale bar = 5 cm

to represent beach foreshore. Parallel laminae can form both under traction current and wave, but in association with ripple-forms draped by sandstone laminae, the balance tilts towards wave. The channel facies TUb, with shore-parallel ripple orientation, is reasonably correlated with longshore troughs in the same association. Lateral interchanges between ripple laminae and planar laminae reflect unsteadiness within individual flows. On the other hand, the grain-size variation between different channel-fills reflects the flow intensity variation between longshore currents. The ripple climbs in some channel-fills of facies TUc indicate a significant fall-out rate of the suspension (Jopling and Walker 1968). While the facies TUc possibly represents a fair-weather condition, and, the large-scale coarse-grained HCS sandstone facies TUd appears to record seasonal storms. The sea-surface rise during seasonal storms can account for the local onlapping of the transgressive lag of this facies (Harms et al. 1982). The wavy-laminated fine-grained sandstones possibly record the upward transition from the facies TUd to the facies TUe and the transition from storm to fair-weather condition. The large-scale trough-cross-stratified granule- and shell-bearing sandstone facies TUf presumably represents a bar that belongs to the breaker zone. In the close neighborhood, the large-scale tabular cross-stratified facies TUg, often in climbing sets, also appears as a bar. The reason for the decrease in the cross-stratified thickness of climbing sets is subcritical climb of dunes. These bars might belong to the same breaker zone, but seemed to locate comparatively distal part from the shoreline with respect to the facies TUf, judging by the comparatively finer grain-size in their composition. Consistent shoreline-parallel orientation of the current suggests that the longshore current dominated the depositional setting of the upper shoreface assemblage. Rapid lateral facies transitions within the upper shoreface assemblage suggest irregularities of palaeoshoreline configuration caused presumably by mega cusps indented by major storms.

Appearance of mudstone beds in the TL subdivision is some kinds of signals for general decline in flow velocity. Intense bioturbation in the mudstone facies TLa also indicates a general decline of the sedimentation rate (Howard 1975). The horizontal infaunal burrows discard the possibility of severe restriction in oxygen supply. The almost gradational upward passage of this mudstone facies TLa to the fine-grained tabular-cross-stratified sandstone facies TLb suggests the transition from below wave base to above wave base. Scarcity of burrows in the sandstone facies TLb is attributable to the current agitation, which hindered the settling of burrowers (Howard 1975; D'Alessandro and Bromley 1987). The fine-grained HCS sandstone facies TLc is inferred as storm deposit. The TL subdivision of the shoreface assemblage is interpreted here as of the lower shoreface.

4.3 TST shelf facies assemblage

This facies assemblage composed of shale (TSa), sandstone (TSb) and conglomeratic (TSc) facies. Greenish-gray shale in the lower part and dark-green shale in the upper part of this 15 m-thick assemblage, form sheet or tabular bodies traced over several kilometers (TSa; Fig. 4a). The lower part includes light-colored silt in forms of starved ripples with average amplitude of 3.6 cm, whereas in the upper part, the silt is present in forms of sub-millimeter-thick planar stringers; and the frequency in occurrence of these stringers decreases upward. Bansal et al. (2017) recorded the authigenic glauconite in this facies, and also noted the upward increase in the volumetric proportion of glauconite.

The sandstone facies TSb alternating with the shale facies TSa is also generally of sheet or tabular geometry. The sandstones are fine-grained and well-sorted, but variously stratified. Some composed the chevron cross-stratified sandstone facies TSbi (Fig. 4b), some composed the hummocky cross-stratified sandstone facies TSbii (Fig. 4c), and some others composed the parallel-laminated sandstone facies TSbiii. Hummocky cross-strata often exceed 3 m in wave length. The trough cross-stratified facies TSbiv also occurs in variety, but rarely. Even more rarely, this sandstone facies displays in cross-stratification geometry, changing laterally from steep to gentle (Fig. 4d). The HCS beds are internally overall graded and measured up to 80 cm in thickness, occasionally bearing gutter casts at their base (Fig. 4e) and having sharp bottoms.

Amidst all the aforementioned laterally-extensive beds, there are short lenticular patches that are present within the conglomeratic facies TSc (Fig. 4f). The clasts in these conglomerates are substantially larger than sand grade size, including either shells of benthic bivalves or quartz granules both along with the omnipresent reddish mud. The reddish mud strongly contrasts to the shelf-originated shale in color, and fills the interstitial spaces and shell cavities, including the wide ligament depressions. The clasts constitute a significant volume of the conglomerates, exceeding 30% of the rock volume. The wave or current structures are generally absent within these conglomerates. Evidence of erosion under these conglomerates is seldom present at their base and even where it presents, it is very limited. Average thickness and outcrop length of these conglomerate patches are 18 cm and 1.6 m respectively.

The sandstone–shale ratio measured in successive bed-couplets decreases upward through the two assemblages (Fig. 1). Parasequences are detectable in the

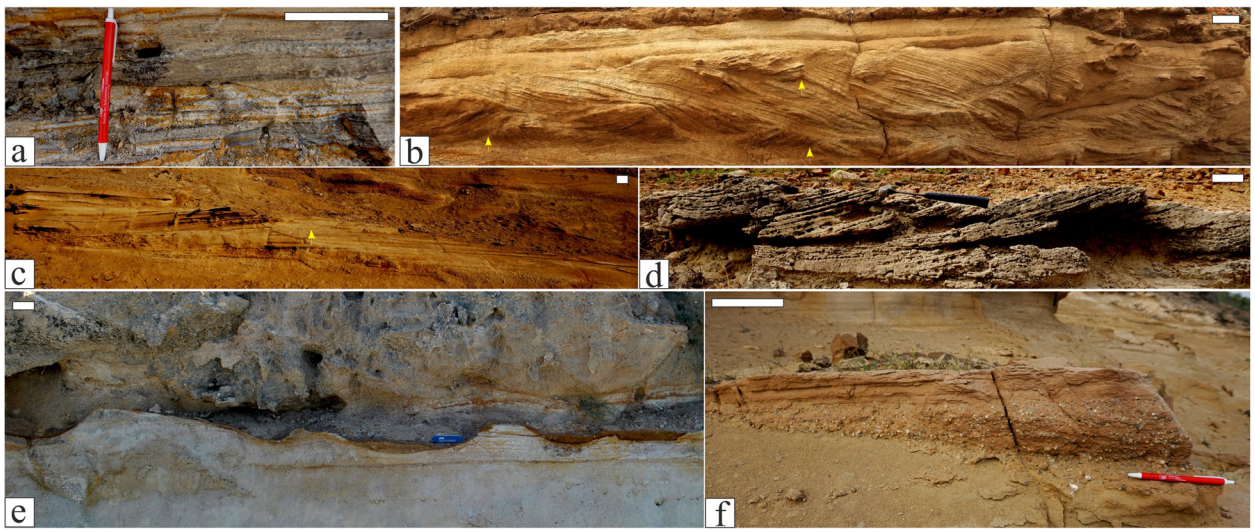

Fig. 4 A TST shelf facies assemblage: **a** Planar-laminated shale facies greenish-gray in lower part, turning dark-green in upper part; **b** Chevron cross-strata (arrows) in well-sorted sandstone facies; **c** Well-sorted hummocky cross-stratified sandstone facies; **d** Cross-stratification changing laterally from steep to gentle in a sandstone facies; **e** Sharp base of a HCS bed with gutter casts; **f** Conglomerate facies, wedge-shaped body with flat base and convex-up top (center). Scale bar = 10 cm

resultant curve and their thickness overall decreases upward (Fig. 1).

4.3.1 Interpretation

The facies TSa of the TST shelf facies assemblage is distinctly finer-grained than the preceding assemblage, and the shale in this assemblage is gray to greenish-gray in color unlike the red mudstone in the inferred shoreface assemblage. In consistency with the previous interpretation, this assemblage is therefore inferred to be deposited on the shelf. The sedimentary structures in the sandstone beds clearly depict dominance of wave-imprint. Tidal imprints are recorded only in the trough cross-stratified facies (TSbiv) in which cross-strata geometry changes laterally. However, any cyclicity in the change could not be established because of exposure limitation. The beds with meters-length HCS are likely to be generated by seasonal storms (Harms et al. 1982; Bose and Chanda 1986). The shale facies TSa is, in contrast, a fair weather product. Against this background, the facies TSc generally lacks in wave or current structures as well as the lateral continuity, and are considered as fluxoturbidites. The three major constituents of these fluxoturbidites, the granules, the bivalve shells and the red interstitial mud, are apparently derived from the shoreface. The overall upward decreasing trend in the sandstone–shale ratio through the shelf facies assemblage superposed on the shoreface facies assemblage corroborates the interpretation of gradual deepening and TST formation (Bansal et al. 2017). Color variation and variable silt inclusion in the shales also support the contention of gradual deepening of the sea.

4.4 HST shelf facies assemblage

This facies assemblage of about 44 m thick is made of sandstones and shales, and directly overlies the preceding assemblage. It is bounded below by a bed of glauconite-rich greenish-black shale, presumably of the maximum flooding zone; and is bounded above by a blanket of conglomerate at the base of the Upper Terrestrial Member which is mainly fluvial in origin (Mandal et al. 2016). This assemblage is best exposed at Lakhpat (L3). Bansal et al. (2017) noted a sharp decline in glauconite content in this assemblage.

Shale facies (HSa) frequently occurring in the lower part of this assemblage, appears more or less homogenous, and dark gray in color. Locally, the facies HSa is planar-laminated, and its thickness can be up to 90 cm (Fig. 5a). Amalgamation of successive shale beds in some of the units becomes apparent from the preferred concentration of burrows at certain levels. A silty-shale facies (HSb) ca.80 cm thick, locally superjacent to the preceding facies HSa (Fig. 5b), is also present in the lower part of this assemblage. This facies is a bit lighter in color because of the presence of numerous silty ripples within the dark-colored shale, together giving rise to lenticular beddings (Reineck and Singh 1973). The average amplitude and wavelength of the ripples are 1 cm and 3.5 cm respectively. Vertical burrows occur infrequently within the ripples. Most of the burrows reflect the escaping activity of burrowers. The laminae around the burrows are discernibly deformed in many instances. Relatively sandstone-rich sandy shale facies (HSc, maximum thickness ca.55 cm) also occurs within this assemblage. This facies is

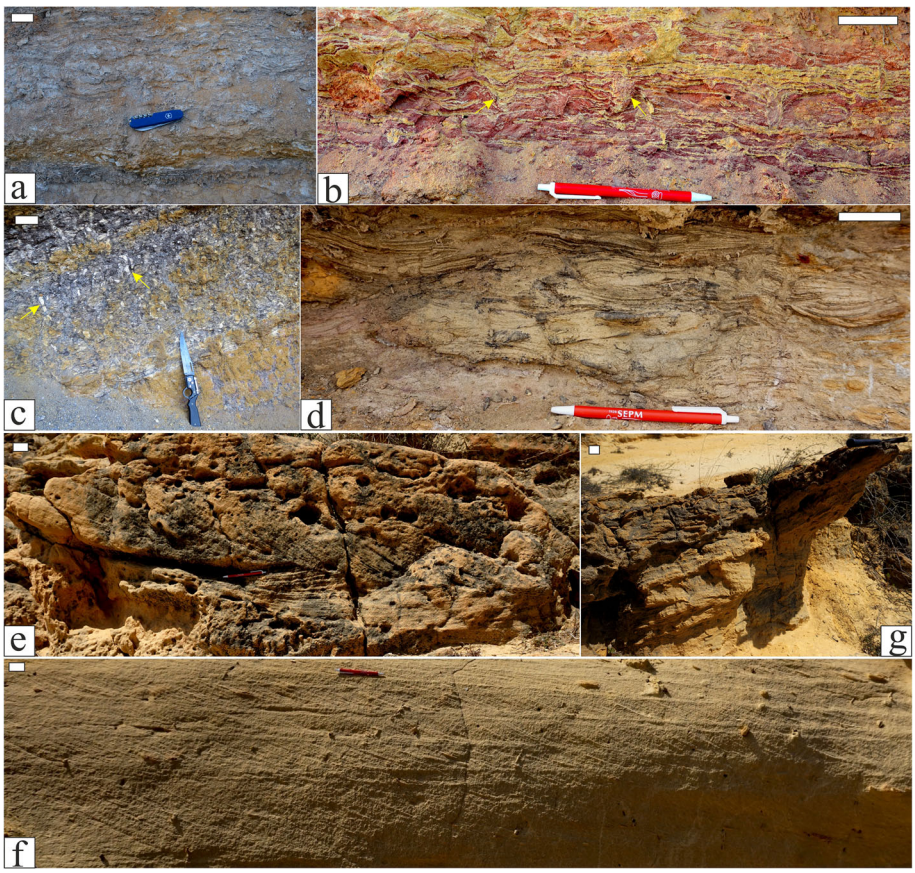

Fig. 5 A HST shelf facies assemblage: **a** Dark-gray shale facies overlying the maximum flooding zone; **b** Comparatively lighter-colored shale encasing starved siltstone ripples. Note escape burrows (arrows) and discernible deformation of strata around them; **c** Sandy shale facies still lighter in color because of buff-colored sandstone ripples encased by dark shale laminae. Note vertical sand-filled burrows (arrows) with mud linings; **d** Shaly sandstone facies in which mud accumulated preferably within the troughs of the sandy ripples. Note mud drapes on the ripple laminae too; **e** Herringbone cross-stratified sandstone facies; **f** Compound cross-stratified facies; **g** Parasequence, Fe-encrusted on top (hammer on top). Scale bar = 5 cm

comparatively lighter in color because of the presence of buff-colored sandstone ripples, giving rise to lenticular beddings. Both vertical and horizontal burrows are frequently present (Fig. 5c). The burrows often have muddy linings. The next coarse facies is shaly sandstone facies (HSd). The sandstone forms starved ripples, and the mudstone preferably occurs in troughs of the ripples, together giving rise to flaser beddings (Fig. 5d; Reineck and Singh 1973). Mud drapes occur also on top of the cross-laminae. The ripples have an average height of 1.2 cm and an average spacing of 4 cm. Vertical and/or oblique burrows, also with dark mud linings, are common in occurrence in this facies. The burrows have a maximum length of about 27 cm and an average diameter of 2 cm. Some individual units of this facies are measured up to 1.2 m in thickness.

The fine-grained sandstone facies HSe, characterized by the herringbone cross-strata (Fig. 5e), is rare in occurrence. Thicknesses of the cross-strata in this facies are less than 60 cm. The coarse-grained sandstone facies characterized by the compound cross-strata (HSf; Fig. 5f), tabular cross-strata (HSg), and large and small trough cross-strata (HSh and HSi). The larger trough cross-strata are often thicker than 60 cm. Mud drapes on the foreset are commonplace that enhance to create the lateral change in cross-stratification style. The sandstone facies HSj is planar-laminated, and burrows are rare in occurrence. The burrows present in this assemblage are dominantly vertical and on many instances have mud-linings; meanwhile, the horizontal echinoid burrows occur more often.

This HST shelf facies assemblage is made of successive depositional cycles, which are coarsening and thickening upward (Fig. 1). Each cycle boundary is conspicuously demarcated by iron encrustation (Fig. 5g). The ratio of sandstone to shale through them increases overall upward (Fig. 1).

4.4.1 Interpretation

In contrast to the wave imprints in the preceding assemblage, only unidirectional cross-strata develop in this assemblage. The cross-strata often organize in forms of herringbone, flaser, and lenticular beddings, revealing the dominance of tides, instead of waves. Mud drapes on the cross-strata further corroborate this contention (De Raaf and Boersma 1971; Terwindt 1981). It is certain that the deposition took place on a tide-dominated shelf. The large-scale compound, tabular and/or trough cross-stratified sandstone bodies presumably represent bars on this tide-dominated shelf. It is also presumed that the mud deposition was dominated in the deeper offshore region, especially in facies HSa and HSb. Quiet water deposition boosted the burrowing activity in these facies. On the other hand, the sandy shale facies HSc is interbedded with sandstones that might deposit in the interbar areas. The sandstone becomes coarsening upward, indicating that the shelf becomes shallow through time. Mud linings of burrows in sandstones attest a significant increase in depositional energy. The upward increasing sandstone-shale ratio in this facies assemblage further corroborates the increase in depositional energy concomitant to the shallowing of the shelf (Fig. 1). This assemblage is inferred to be a HST, resting on top of a TST (Bansal et al. 2017). The coarsening upward depositional cycles within this HST are thus inferred as a parasequence. The iron encrustation formed at the top of the parasequence is possibly caused by the significant drop of sedimentation rate during marine flooding period. The sandstone-shale ratio, as can be predicted, overall increases upward through this inferred HST (Fig. 1).

5 Intrinsic details of conglomeratic facies TSc

This conglomeratic facies is inordinately coarser grained than the associated facies on the TST shelf as well as those on the shoreface. In contrast to the general well-sorted nature of other shelf sediments, this facies is polymodal in grain-size distribution. Being comparatively weathering resistant, this conglomeratic facies is prone to exposure and demonstrably retain bed-geometry in the majority of cases. It does not show preference for any lithologic association, neither has any stratigraphic level preference within the TST shelf. All three of their major components, viz., the shells, the granules and even the reddish mud can be traced into the shoreface assemblage. The fossils are left valves of low-diversity bivalve shells, generally thick and sturdy, and have their outer surfaces remarkably roughened with pustules, protruding ridges, well pronounced growth rims and spines, and are generally little damaged. Wide resilifer is also an essential characteristic of these bivalves. There is, however, wide variability in bed geometry, structure and texture between the conglomerate beds belonging to this facies, as described below.

Some internally massive conglomerate bodies are distinctly wedge-shaped having flat base and pronounced convex-up top (subfacies TSc❶; Fig. 6a). Their conspicuous constituents are shells and reddish muddy sandstones filled the interstitial spaces. The shells are chaotically arranged, although the majority of them are oriented convex-up. However, the clast-size discernibly drops at the down-wedge tip of the conglomerate bodies.

Some other conglomerates are characterized by very high concentration of shells in most parts except in a cm-thick basal zone at their base. Their bases are sharp and planar, but geometry of their tops is indeterminable because of weathering. The most remarkable internal feature within these bodies is pronounced coarse-tail reverse grading, manifested in shell size. It is remarkable that the shells are fairly intact (subfaciesTSc❷; Fig. 6b).

Unlike the preceding two kinds, some conglomerate bodies are matrix-supported, with fossils floating in the muddy sandstone matrix (subfacies TSc❸). Also the majority of bioclasts are broken and about 50% of the shells are concave-up in orientation. What is especially remarkable is that the clast distribution depicts coarse-tail normal grading. The conglomerate bodies seem to be of tabular geometry, although weathered incomplete exposure prevents exact reconstruction of their bed geometries (Fig. 6c).

Some conglomerate bodies are clast-supported, although interstitial spaces between the shells and the granules are filled-up by reddish muddy matrix (subfacies TSc❹). The most distinguishable feature of this type of conglomerate is presence of pronounced sets of unidirectional cross-strata. The shells in these beds are mostly convex-up in orientation. The base of the sediment-body is sharp and planar, but its weathered top reveals little about its geometry. The shells are surprisingly unbroken (Fig. 6d).

Still some other conglomerates are made of very poorly-sorted granules measuring up to 9 mm in diameter, while reddish mudstone fills their interstices (subfacies TSc❺). These conglomerates have both flat bottoms and flat tops, although wedging on the flanks. Maximum outcrop length of about 5 m has been noted for these conglomerate bodies. They have cross-strata inside and these cross-strata become progressively more pronounced in the down-dip direction (Fig. 6e). The cross-strata appear to be low angled, around 18°.

Some of the conglomerate bodies are made almost entirely of granules, but have extremely poor sorting owing to the presence of abrupt reddish muddy sandstone matrix within interstices; minute shell hash is locally

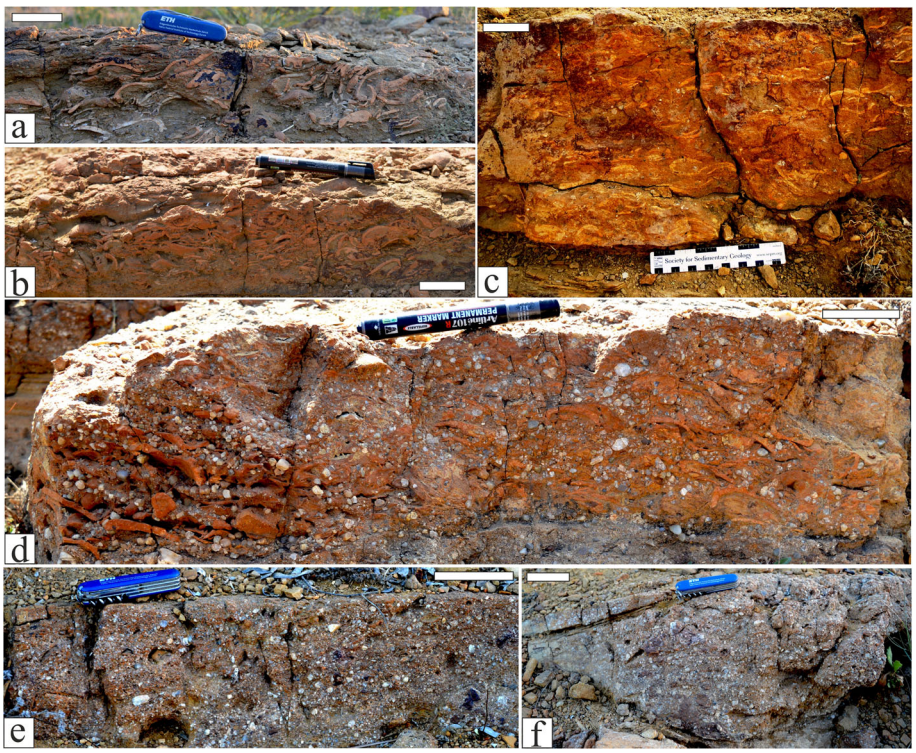

Fig. 6 **a** Wedge-shaped clasts supported fossil-rich conglomerate. Note downcurrent fining of the clasts and also fairly intact nature of the shells; **b** Clast-supported conglomerate displaying coarse-tail reverse grading. Note lack of discernible skeletal materials at the base. Also note the shells are fairly intact; **c** Matrix-supported conglomerate, with tabular geometry. Note that the majority of shells are concave-up in orientation, present normal coarse-tail grading. Also note many shells are broken; **d** Clast-supported conglomerate showing faint cross-strata as internal structure. Note that majority of shells are convex-up in orientation, although majority of them are fairly intact; **e** Granule-rich and very poorly-sorted conglomerate, with reddish mud filling the interstices between the clasts. Note that the cross-strata within them turn progressively more pronounced in the down-dip direction; **f** Granule-rich and very poorly-sorted conglomerate, having concave-up base with flat top. Note internally the sediment appears massive but with a faint suggestion of internal lamination. Scale bar = 5 cm

detected (subfacies TSc❻). These conglomerate bodies form biconvex lenses. Granule diameter measures up to about 7 mm, but distinctly decreases sharply on the flanks. Otherwise these conglomerates appear massive in most cases; but on some instances, there is a faint suggestion of internal laminae. The bases of these conglomerate bodies are concave upward with tops, more or less, suggesting flat channel-forms (Fig. 6f).

5.1 Interpretation

The conglomerate bodies of the subfacies TSc❶ resemble small fans (Gruszczyński et al. 1993). The pronounced convexity of the top surface of the massive pile suggests that the sediment-driving flow earned high viscosity prior to deposition. Fairly intact nature of the pelecypod valves corroborates this contention. Chaotic arrangement of the shells, however, suggests turbulence in the flow immediately before turning viscous. Considering all the aspects stated above, the deposition seems to have taken place rapidly because of freezing of the matrix; and, a hydraulic jump at the base of a slope can be envisaged (Fisher 1983).

Reverse grading in the subfacies TSc❷, despite presence of intergranular matrix, strongly suggests operation of modified grain-flow mechanism for sediment transport immediately prior to deposition (Middleton and Hampton 1976). The very sharp but planar basal surface of most of these conglomerate bodies is in agreement with this mechanism. It appears that the heavily loaded flow created a strong shear on the depositional surface. The dispersive pressure, created thereby, pushed the clasts upward; and, the larger the clast was, the higher it was pushed up (Middleton 1976). High concentration of shells makes the frequent near-collision between shells conceivable readily; then the reverse grading arose in consequence. Sediment settling presumably initiated from the top of the flow and extended downward; fluidity persisted longest at the base of the flow because of the basal friction (Middleton 1967). Rarity of identifiable shells at the base of the beds corroborates this assumption of strong shear at the flow base. The flow is testified

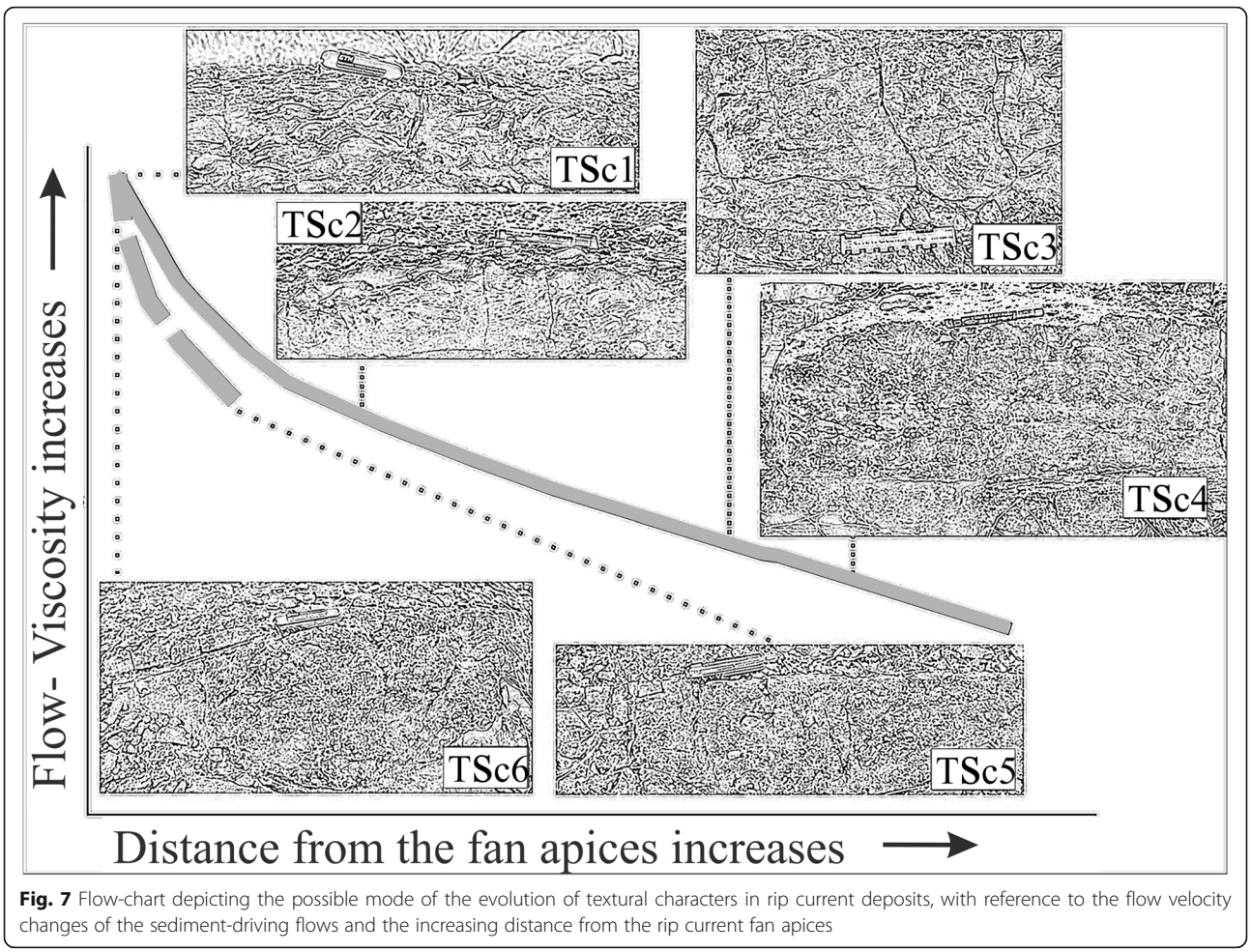

Fig. 7 Flow-chart depicting the possible mode of the evolution of textural characters in rip current deposits, with reference to the flow velocity changes of the sediment-driving flows and the increasing distance from the rip current fan apices

viscous as the limited breakage of shells, but its viscosity is comparatively lesser than that of the flow depositing the preceding group of massive beds.

In comparison to the previous two cases, the normally graded conglomerate subfacies TSc❸ have presumably been products of the flow even more fluidal. Normal grading suggests comparatively greater fluidity in the flow as it allowed coarse clasts to settle first. This fact is further corroborated by the oriented concave-up shells, settling from suspension. In good agreement to this contention of flow turbulence, the shells are broken.

The cross-stratified conglomerate subfacies TSc❹ appears to be products of bed-form migration that took place under the influence of unidirectional light-density currents. The flow was highly turbulent so it did not allow much of the sand-sized or smaller particles to settle; and towards the downcurrent, the clasts have decreased in size. However, the low degree of shell breakage creates a snag, especially in contrast to the high degree of shell breakage within the immediately preceding graded facies. It is possible that the transport might be short so the deposition took place close to the shell bank. And then, both the granules as well as the shells in these conglomerates could be inferred to come from the same locality. Like the large size of the granules, the surface roughness of the shells also indicates a source of sediment in a highly turbulent zone. The source could be the breaker zone, close to the marine shelf where the deposition took place. The shells were apparently derived from shell banks developed in the breaker zone. It can be recalled that some bars in the shoreface assemblage do contain the granules as well as the shells of similar size.

Massive and poorly-sorted subfacies TSc❺ still indicates a rapid deposition. The flat top and the low angle of cross-strata identify the facies body laterally-accreting and fan-like. The rapid dumping of sediment can be attributed to a hydraulic jump. This facies is likely to be a product of the sudden flow expansion, beyond the constricted mouth of channels, which is similar to that accommodated with the preceding facies. This facies is thus interpreted as a downcurrent counterpart of the subfacies TSc❻.

The subfacies TSc❻ apparently fills narrow channel cuts. The poorly sorted, massive nature of the erosional channel fills indicates rapid deposition. Distinct convexity of the top of the conglomerate bodies attest to the considerable viscosity of the flow, although the erosional cuts at their base indicate the turbulence. The deposition might take place at the base of a slope. Significant hydraulic jump might cause a rapid freezing of the flow, as it happens in case of debris flows. This assumption provides a satisfactory explanation for the convexity of the top of the bodies.

The textural differences between the subfacies of facies TSc can be explained by the flow velocity changes, related to the changes in the depositional slope, the amount of fluid incorporation, and the travelled distance from the fan apices (Fig. 7).

6 Recognition of rip currents

The conglomerates amidst the fine-grained facies bear signature of episodic enhancement of depositional energy more than what seasonal storms used to instill. Seismicity as the triggering mechanism for their involvement can be ruled out because of lack of lateral continuity and stratigraphic selectivity in occurrence within the TST stratigraphy. Continuation of the same palaeogeography across the conglomerates further denies their genetic relationship with seismicity. Cessation of rifting long before initiation of the major transgression that led to formation of the Ukra Member also supports this contention (Biswas 2016b). On the other hand, the offshore-directed cross-strata data in these conglomerates against the background of shore-parallel current domination in the TST, strongly suggests the offshore delivery of shoreface materials by stronger flow than those driven by seasonal storms, like typhoons or tsunamis, which are known to enhance rip currents enormously (Picard and High 1968; Kazmierczak and Goldring 1978; Morton 1978; Yang et al. 2017). The dominance of wave structures against nearly non-existent tidal imprints in the TST indicates that the hydrodynamics on the shore of the Ukra Sea had a foreboding of such disastrous storms. On the shoreface, spectral variation in facies composition and rapid transitions between them suggest irregularity of the

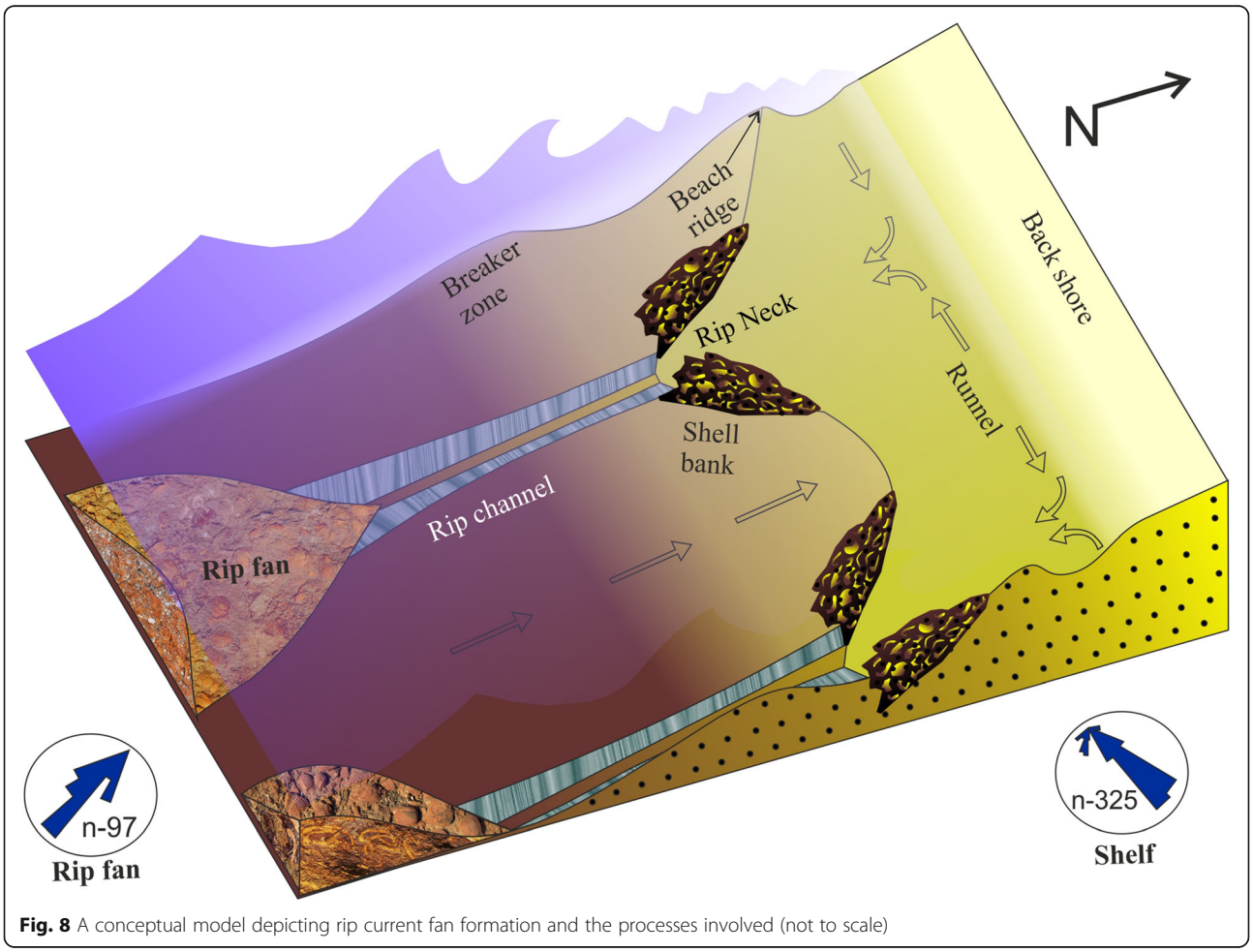

Fig. 8 A conceptual model depicting rip current fan formation and the processes involved (not to scale)

palaeoshoreline presumably for formation of mega cusps under the assault of such megastorms (Thornton et al. 2007). Absence of deposits comparable to the facies TSc in the tide-dominated HST provides an indirect support for its interpretation as rip current deposit. Absence of similar deposit in the shoreface assemblage of the TST segment may be attributed to our failure to recognize it because of coarse grain size of the background sediment; distinction of rip current deposit is minimized.

The low population diversity of bivalve fossil within the conglomerates appears to be para-autochthonous. The most favorable site for growth of banks of these sedimentary bivalves should have been the rip-channel necks that most probably used to receive organic matter most readily. Strong rip currents possibly uprooted them (Fig. 8). High turbulence at the channel neck probably winnowed out fine fraction of sediment and concentrated the granules and uprooted shells. On the way to the channel mouth the rip current presumably incorporated reddish mud in plenty as the incoming waves threw them up in suspension.

6.1 Differences between deposits of seasonal storms and rip currents

The differences between deposits of seasonal storms and the purported rip currents within the TST shelf facies of the Ukra Member and their explanations may generate further insights about the latter, seldom identified in ancient successions. The differences and their respective explanations are:

1) Inordinately coarse grain-size of the recognized rip current deposits points to enormous increase in episodic energy input.
2) Exceptional abundance of shells in the majority of inferred rip current deposits is again related to the excessive energy flux in the marine setting. It is possible that seasonal storms were not perhaps sufficiently strong to cause mass destruction of the shell banks. Also, the shells in the rip currents suffered little abrasion except at the channel neck only where the turbulence was possibly high. It can be visualized that the rip current plumes tended to freeze immediately after they spilled over the incoming waves and landed on the shelf floor (Davis 1978).
3) The inferred rip current deposits are extremely poorly-sorted, but the seasonal storm deposits are well- to moderately-sorted. While light-density currents induced by seasonal storms were amenable to grain sorting, high viscosity of rip currents were not.
4) The unimodality of grain-size distribution in seasonal storm deposits is in contrast to the polymodal distribution of the inferred rip current deposits. Instantaneous deposition of the entire range from granules and large shells to mud of load from the rip currents ensures the polymodality in grain-size distribution.
5) In contrast to the sheet or tabular geometry of seasonal storm deposits, the rip current deposits are lenticular, not exceeding 3 m in outcrop length. The inferred rip current deposits assume lenticular geometry being delivered through constricted channels.
6) Deposits of seasonal storms are generally finely stratified, but those laid by rip currents generally lack stratification. Contrasting flow-density is perhaps responsible for this difference.
7) Massiveness and graded bedding, normal and reverse, are commonplace within alleged rip current deposits, while seasonal storm deposits have only overall graded across stratification. The overall grading in seasonal storm deposits only reflects deposition from waning currents. Massive and graded bedding formation within the rip current deposits follows the doctrine of massflow mechanisms.
8) Base is generally sharper than top in the seasonal storm beds, which presents a contrast with the both sharp contacts in rip current-originated bodies, except in normally graded beds. Waning of the flows generated by seasonal storms and rapid freezing of rip-current-induced flows create the difference.
9) Bed load movement in seasonal storm deposits often manifests wave action in internal structures; whereas bed load movement, if at all arises in rip currents, gives rise to unidirectional cross-strata.
10) Current structures at the sole of beds are common when the depositional agent is seasonal storms, but rare when the agent is rip currents. This difference arises from the general lack of turbulence in rip currents at the channel mouth, because at the channel mouth, rip currents override the incoming waves (MacMahan et al. 2006). In one outcrop of the Ukra Member, between two inferred rip-current fan-clinoforms, a set of mega-ripple laminae occurs in upslope direction possibly bearing testimony to such shoreward upwelling of waves (Fig. 9).

7 Discussion

Exclusive occurrence of ancient rip current records in TST shelf facies, not only within the Ukra Member, but also within the other seven examples we could trace in

Fig. 9 Rip current fan with mega-ripple (arrow) laminae having orientation opposite to the direction of inclination of the fan-clinoforms. Hammer length = 34 cm

the geological literature, has a clear palaeoclimatic implication (Fig. 10). Open shorelines formed during marine transgressions are generally wave-dominated and the waves intensify longshore currents. Long period waves like typhoons/hurricanes and tsunamis further intensify the longshore currents and as a corollary, intensify the rip currents enormously. Wide coastal zones are devastated, mega cusps are formed, and strong rip currents transport distinctively coarse materials from the coastal zone to the offshore (Gruszczyński et al. 1993; Dalrymple et al. 2011). There is no wonder that all the ancient rip current deposits that we could trace are from TSTs or global warming episodes and are likely to have witnessed many typhoons and hurricanes. Global warming creates conditions that facilitate formation of these long period waves more frequently and more intensely. It is a widely held perception that global warming intensifies cyclones and makes them frequent (Gaertner et al. 2009; Mann et al. 2009; Knutson et al. 2010; Mendelsohn et al. 2012; Nissen et al. 2014; Yang et al. 2017). The basic premise of this contention is that when ocean surface temperature increases, a strong vertical shear develops in wind because the upper stratum of atmosphere still remains cool and this shear feeds the storms (Dare and McBride 2011). It follows that TSTs of Earth's warm periods hold better condition for locating rip current deposits. This contention does not, however, mean that colder periods are devoid of rip current records. Korean Peninsula suffered from active typhoons was also in colder periods between 1392 and 1903 (Yang 2010; Katsuki et al. 2016; Yang et al. 2017). There is, nonetheless, an urgent need to have greater knowledge on features of ancient rip current deposits and their depositional modes in view of the present trend of global warming. Emanuel (2005) estimated that Atlantic hurricanes are now approximately 60% more powerful than those that occurred in the 1970s. Sugi et al. (2002) used Global JMA model and Shu (2015) deployed the EC-Earth model of Haarsma et al. (2013) to predict intensification of tropical hurricanes through recent times of global warming. Numerical modeling of Sobel et al. (2016) more recently strengthened that increasing greenhouse gas accumulation in the atmosphere is bound to intensify tropical hurricanes. It is predicted that in the near future rip currents will progressively make sea coasts more dangerous to bathers and increasingly demolish the private properties and tourist facilities built up along sea coasts throughout the world. Typhoon Haiyan in 2015 killed at least 63,000 people and caused property loss in a scale of $4.55 billion (USD) in the Philippines alone. The present Ukra rip current record assumes special importance as it comes from a geological period when the nature itself experienced global warming. More rip current records from the Cretaceous would be especially relevant for assessing the extent of damage we may face in near future, unless steps are taken to arrest and then reverse the trend.

8 Conclusions

Delivery of the coarsest fraction of shoreface sediments by enormously intensified rip currents gave rise to isolated conglomerate patches disrupting the generally fine-grained motif of the TST shelf facies of the Lower Cretaceous Ukra Member, India. Quartz granules and sturdy shells of sedentary bivalves as well as reddish mud constituted this fraction. High

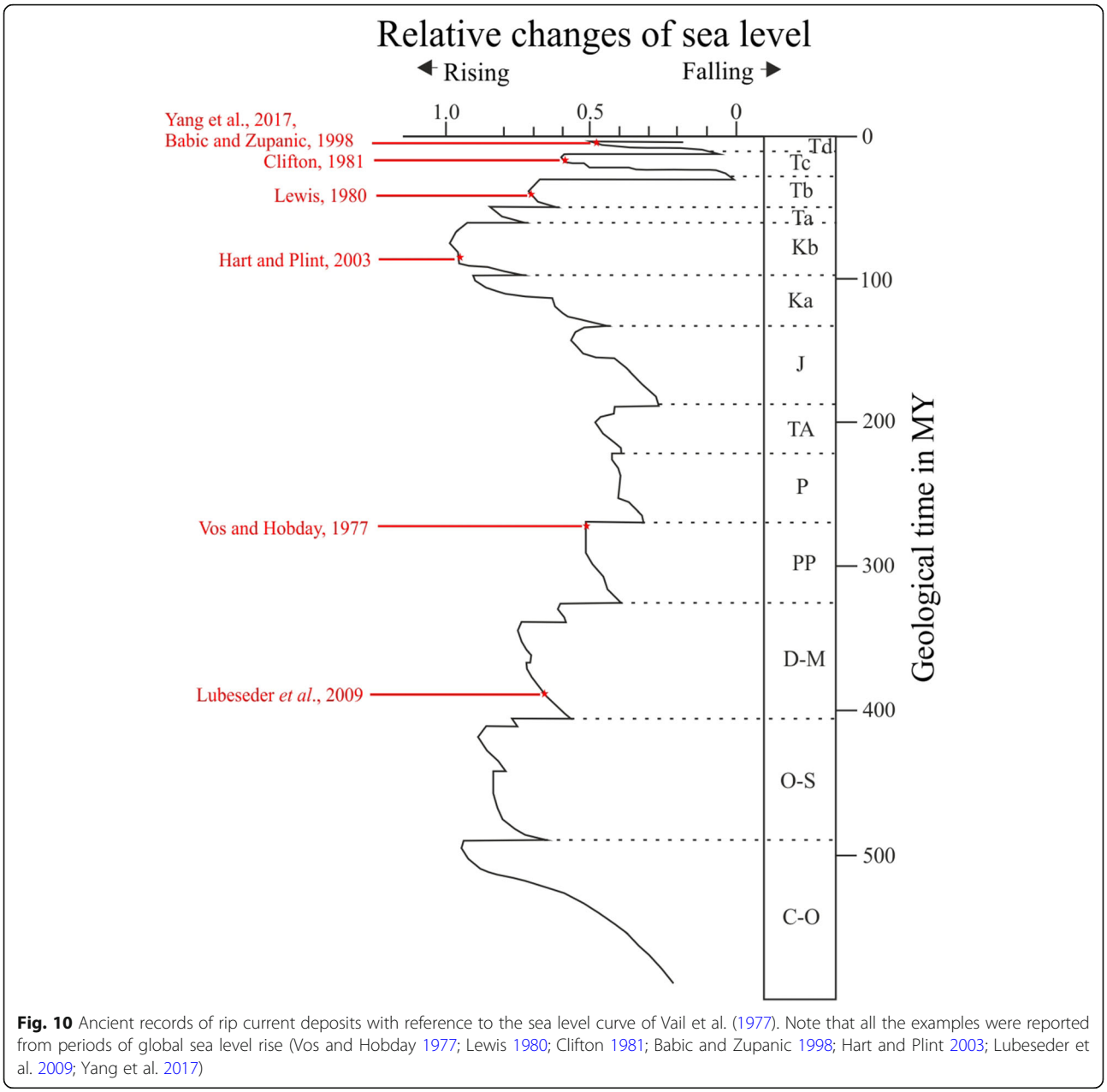

Fig. 10 Ancient records of rip current deposits with reference to the sea level curve of Vail et al. (1977). Note that all the examples were reported from periods of global sea level rise (Vos and Hobday 1977; Lewis 1980; Clifton 1981; Babic and Zupanic 1998; Hart and Plint 2003; Lubeseder et al. 2009; Yang et al. 2017)

turbulence at the neck of rip current channels concentrated the granules and extensively damaged the bivalve banks at the same site. However, admixture with shoreface-derived reddish mud made the conglomerates poorly-sorted and matrix-supported in the majority of cases. Deposition from suspension had become a rule as rip currents rode over the incoming waves at the channel mouths. Mass flows of different viscosities operated immediately prior to deposition unless incorporation of seawater made the rip currents fluidal and turbulent. Consequently the rip current deposits in the Ukra Member formed small fan-like bodies, generally having flat base and convex-up top. These rip current fans in the Ukra Member, like all known ancient counterparts, formed during a phase of global warming, resultant intensification of storms and consequent strengthening of longshore currents. These rip current deposits laid by mega storms have distinctive characteristics with respect to the products of seasonal storms. The ancient rip current deposits, therefore, stand as valuable proxies for researching the palaeoclimate.

Abbreviations

HCS: Hummocky cross-stratified; HST: Highstand systems tract; MFZ: Maximum flooding zone; TST: Trangressive systems tract

Acknowledgements
Both the authors are indebted to Pradip K Bose for a pre-submittal review of a previous version of this manuscript and encouragement. Both the authors appreciate the infrastructural help they received from the Department of Geological Sciences, Jadavpur University, Kolkata, India.

Authors' contributions
SS and AK carried out the fieldwork and data collection in the field. SS helped to make the first draft of the manuscript. AK made the literature survey. The authors read and approved the final manuscript.

Funding
For financial help SS gratefully acknowledges the Council of Scientific and Industrial Research (CSIR) Government of India sponsoring the Project No. 24(0336)/14/EMR-II; and AK acknowledges the Department of Science and Technology (DST) Government of India sponsoring an Inspire Fellowship.

Availability of data and materials
Information of data and material(s) is in figures and within the manuscript.

Competing interests
The authors declare that they have no competing interests.

Received: 1 August 2019 Accepted: 23 March 2020
Published online: 23 April 2020

References

Arthur, R.S. 1962. A note on the dynamics of rip currents. *Journal of Geophysical Research* 67 (7): 2777–2779.

Babic, L., and J. Zupanic. 1998. Nearshore deposits in the middle Eocene clastic succession in northern Dalmatia (Dinarides, Croatia). *Geologia Croatica* 51 (2): 175–193.

Bansal, U., S. Banerjee, K. Pande, A. Arora, and S.S. Meena. 2017. The distinctive compositional evolution of glauconite in the cretaceous Ukra Hill member (Kutch Basin, India) and its implications. *Marine and Petroleum Geology* 82: 97–117.

Basco, D.R. 1983. Surf zone currents. *Coastal Engineering* 7: 331–355.

Birkemeier, W.A., and R.A. Dalrymple. 1975. *Nearshore water circulation induced by wind and waves*. In *Procedure symposium on modelling technique*, 1062–1081. New York: American Society of Civil Engineering.

Biswas, S.K. 1977. Mesozoic stratigraphy of Kutch, Gujarat. *Quarternary Journal of Geological Mineralogical and Meteorological Society of India* 49 (3–4): 1–52.

Biswas, S.K. 1987. Regional tectonic framework, structure and evolution of the western margin basins of India. *Tectonophysics* 135: 307–327.

Biswas, S.K. 1991. Stratigraphy and sedimentary evolution of the Mesozoic Basin of Kutch, Western India. In *Sedimentary basins of India, tectonic context*, ed. S.K. Tandon, C.C. Pant, and S.M. Casshyap, 74–103. Nainital: Gyanodaya Prokashan.

Biswas, S.K. 2016a. Tectonic framework, structure and tectonic evolution of Kutch Basin, Western India. *Special Publication of the Geological Society of India* 6: 129–150.

Biswas, S.K. 2016b. Mesozoic and tertiary stratigraphy of Kutch (Kachchh) –– A review. *Special Publication of the Geological Society of India* 6: 1–24.

Bose, P.K., and S.K. Chanda. 1986. Storm deposits and hummocky cross-stratification: A geological viewpoint. *Quarternary Journal of Geological Mineralogical and Meteorological Society of India* 58 (1): 53–68.

Bose, P.K., S. Shome, S. Bardhan, and G. Ghosh. 1986. Facies mosaic in the Ghuneri member (Jurassic) of the Bhuj formation, western Kutch, India. *Sedimentary Geology* 46: 293–309.

Bowman, D., D. Arad, D.S. Rosen, E. Kit, R. Goldbery, and A. Slavicz. 1988b. Flow characteristics along the rip current system under low energy conditions. *Marine Geology* 82: 149–167.

Bowman, D., D.S. Rosen, E. Kit, D. Arad, and A. Slavicz. 1988a. Flow characteristics at the rip current neck under low energy conditions. *Marine Geology* 79: 41–54.

Clarke, L., D. Ackerman, and J. Largier. 2007. Dye dispersion in the surf zone: Measurements and simple models. *Continental Shelf Research* 27: 650–669.

Clifton, H.E. 1976. Wave formed sedimentary structures, a conceptual model. *SEPM Special Publication* 24: 126–148.

Clifton, H.E. 1981. Progradational sequences in Miocene shoreline deposits, southeastern Caliente range, California. *Journal of Sedimentary Reasearch* 51 (1): 165–184.

D'Alessandro, A., and R.G. Bromley. 1987. Meniscate trace fossils and the Muensteria-Taenidium problem. *Palaeontology* 30: 743–763.

Dalrymple, R.A., J.H. MacMahan, A.J.H.M. Reniers, and V. Nelko. 2011. Rip currents. *Annual Review of Fluid Mechanics* 43: 551–581.

Dare, R.A., and J.L. McBride. 2011. The threshold sea surface temperature condition for tropical cyclogenesis. *Journal of Climate* 24 (17): 4570–4576.

Davidson-Arnott, R.G.D., and B. Greenwood. 1974. Bedforms and structures associated with bar topography in the shallow-water environment, Kouchibouguac Bay, New Brunswick, Canada. *Journal of Sedimentary Petrology* 44: 698–704.

Davidson-Arnott, R.G.D., and B. Greenwood. 1976. Facies relationships on a barred coast. In *Beach and nearshore sedimentation*, ed. R.A. Davis and R. L. Ethington, vol. 24, 140–168. New Brunswick: SEPM Special Publication.

Davis, R.A.J.R. 1978. *Coastal sedimentary environments*, 420. Berlin: Springer-Verlag.

De Raaf, J.F.M., and J.R. Boersma. 1971. Tidal deposits and their sedimentary structures. *Geologie en Mijnbouw* 50 (3): 479–504.

Emanuel, K. 2005. Increasing destructiveness of tropical cyclones over the past 30 years. *Nature* 436: 686–688.

Fisher, R.V. 1983. Flow transformations in sediment gravity flows. *Geology* 11: 273–274.

Fürsich, F.T., and D.K. Pandey. 2003. Sequence stratigraphic significance of sedimentary cycles and shell concentrations in the upper Jurassic–lower cretaceous of Kachchh, western India. *Palaeogeography Palaeoclimatology Palaeoecology* 193: 285–309.

Gaertner, M.A., M. Domínguez, V. Gil, and E. Sánchez. 2009. Risk of tropical cyclones over the Mediterranean Sea in a change scenario. In *Hurricanes and climate change*, ed. J.B. Elsner and T.H. Jagger, 235–250. New York: Springer US.

Grant, S., J.H. Kim, B.H. Jones, S.A. Jenkins, and J. Wasyl. 2005. Surf zone entrainment, along-shore transport, and human health implications of pollution from tidal outlets. *Journal of Geophysical Research* 110: C10025.

Greenwood, B., and R.G.D. Davidson-Arnott. 1979. Sedimentation and equilibrium in wave formed bars: A review and case study. *Canadian Journal of Earth Science* 16: 312–332.

Greenwood, B., and P.B. Hale. 1980. Depth of activity, sediment flux and morphological change in the barred nearshore environment. In *The coastline of Canada*. Geological Survey of Canada 80 (10), ed. S.B. McCann, 89–109.

Gruszczyński, M., S. Rudowski, J. Semıl, J. Słomiński, and J. Zrobek. 1993. Rip currents as a geological tool. *Sedimentology* 40: 217–236.

Haarsma, R.J., W. Hazeleger, C. Severijns, H.D. Vries, A. Sterl, R. Bintanja, G.J.V. Oldenborgh, and H.W.V.D. Brink. 2013. More hurricanes to hit western Europe due to global warming. *Geophysical Research Letters* 40: 1783–1788.

Harms, J.C., J.B. Southard, and R.G. Walker. 1982. Structures and sequences in clastic rocks. *SEPM Short Course* 9: 180.

Hart, B.S., and A.G. Plint. 2003. Stratigraphy and sedimentology of shoreface and fluvial conglomerates: Insights from the Cardium formation in NW Alberta and adjacent British Columbia. *Bulletin of Canadian Petroleum Geology* 51 (4): 437–464.

Howard, J.D. 1975. The sedimentological significance of trace fossils. In *The study of trace fossils*, ed. R.W. Frey, 131–146. New York: Springer.

Inman, D.L., and B.M. Brush. 1973. The coastal challenge. *Science* 181: 20–32.

Jopling, A.V., and R.G. Walker. 1968. Morphology and origin of ripple-drift cross-lamination, with examples from the Pleistocene of Massachusetts. *Journal of Sedimentary Petrology* 38 (4): 971–984.

Katsuki, K., D.Y. Yang, K. Seto, M. Yasuhara, H. Takata, M. Otsuka, T. Nakanishi, Y. Yoon, I.-K. Um, R.C.W. Cheng, B.-K. Khim, and K. Kashima. 2016. Factors controlling typhoons and storm rain on the Korean peninsula during the little ice age. *Journal of Paleolimnology* 55 (1): 35–48.

Kazmierczak, J., and R. Goldring. 1978. Subtidal flat-pebble conglomerate from the upper Devonian of Poland: A multiprovenant high-enerhy product. *Geological Magazine* 115 (5): 359–366.

Knutson, T.R., J.L. McBride, J. Chan, K. Emanuel, G. Holland, C. Landsea, I. Held, J.P. Kossin, A.K. Srivastava, and M. Sugi. 2010. Tropical cyclones and climate change. *Nature Geoscience* 3: 157–163.

Komar, P.D. 1976. *Beach processes and sedimentation*, 429. Englewood Cliffs: Prentice Hall.

Krishna, J. 1987. An overview of Mesozoic stratigraphy of Kachchh and Jaisalmer basins. *Journal of Paleontological Society of India* 32: 136–149.

Lenhart, R.J. 1979. *Nearshore marine bedforms, formative processes, distribution and internal structures*Ph.D. Thesis, University of Cincinnati, 166.

Lewis, D.W. 1980. Storm-generated graded beds and debris flow deposits with Ophiomorpha in a shallow offshore Oligocene sequence at Nelson, South Island, New Zealand. *New Zealand Journal of Geology and Geophysics* 23 (3): 353–369.

Longuet-Higgins, M.S., and R.W. Stewart. 1962. Radiation stress and mass transport in gravity waves with application to surf beats. *Journal of Fluid Mechanics* 13: 481–504.

Lubeseder, S., J. Redfern, and L. Boutib. 2009. Mixed siliciclastic-carbonate shelf sedimentation—Lower Devonian sequences of the SW anti-atlas, Morocco. *Sedimentary Geology* 215: 13–32.

MacMahan, J.H., J. Brown, E. Thornton, and A. Reniers. 2010. Mean Lagrangian flow behavior on an open rip-channeled beach: A new perspective. *Marine Geology* 268: 1–15.

MacMahan, J.H., E.B. Thornton, and A.J. Reniers. 2006. Rip current review. *Coastal Engineering* 53 (2–3): 191–208.

Mandal, A., A. Koner, S. Sarkar, H.A. Tawfik, N. Chakraborty, S. Bhakta, and P.K. Bose. 2016. Physico-chemical tuning of palaeogeographic shifts: Bhuj formation, Kutch, India. *Marine and Petroleum Geology* 78: 474–492.

Mann, M.E., J.D. Woodruff, J.P. Donnelly, and Z. Zhang. 2009. Atlantic hurricanes and climate over the past 1,500 years. *Nature* 460: 880–883.

Marchesiello, P., R. Benshila, R. Almar, Y. Uchiyama, J.C. McWilliams, and A. Shchepetkin. 2015. On tridimensional rip current modelling. *Ocean Modelling* 96: 36–48.

McKenzie, P. 1958. Rip currents systems. *Journal of Geology* 66: 103–113.

Mendelsohn, R., K. Emanuel, S. Chonabayashi, and L. Bakkensen. 2012. The impact of climate change on global tropical cyclone damage. *Nature Climate Change* 2: 205–209.

Middleton, G.V. 1967. Experiments on density and turbidity currents III. Deposition of sediment. *Canadian Journal of Earth Sciences* 4: 475–505.

Middleton, G.V. 1976. Hydraulic ınterpretation of sand size distributions. *Journal of Geology* 84: 405–426.

Middleton, G.V., and M.A. Hampton. 1976. Subaqueous sediment transport and deposition bysediment gravity flows. In *Marine sediment transport and environmental management*, ed. D.J. Stanley and D.J.P. Swift, 197–218.

Morton, R.A. 1978. Large-scale rhomboid bed forms and sedimentary structures associated with hurricane washover. *Sedimentology* 25: 183–204.

Nissen, K.M., G.C. Leckebusch, J.G. Pinto, and U. Ulbrich. 2014. Mediterranean cyclones and windstorms in a changing climate. *Regional Environmental Change* 14: 1873–1890.

Noda, E.K. 1974. Wave induced nearshore circulation. *Journal of Geophysical Research* 79: 4097–4106.

Picard, M.D., and L.R. High. 1968. Shallow marine currents on the early (?) Triassic Wyoming shelf. *Journal of Sedimentary Petrology* 38 (2): 411–423.

Rajnath. 1932. A contribution to the statigraphy of Kutch. *Quarternary Journal of Geological Mineralogical and Meteorological Society of India* 4 (4): 161–174.

Reineck, H.E., and I.B. Singh. 1973. *Depositional sedimentary environments*, 549. Berlin: Springer.

Reniers, A.J.H.M., J.H. MacMahan, E.B. Thornton, T.P. Stanton, and M. Henriquez. 2009. Surf zone retention on a rip-channeled beach. *Journal of Geophysical Research* 114: C10010.

Rudra, P., and S. Bardhan. 2006. Status of "Trigonia ventricosa" (Bivalvia) from the upper Jurassic–lower cretaceous of Kutch, western India: Kitchin's unfinished synthesis. *Cretaceous Research* 27: 611–628.

Sasaki, T., and K. Horikawa. 1975. Nearshore current system on a gently sloping bottom. *Coastal Engineering in Japan* 18: 123–142.

Sasaki, T., and K. Horikawa. 1978. Observation of nearshore current and edge waves. In *Proceedings of the 16th international conference on coastal engineering*, 791–809. Hamburg: ASCE.

Shepard, F.P. 1936. Undertow, rip tide or 'rip current'. *Science* 84: 181–182.

Shepard, F.P., K.O. Emery, and E.C.L. Fond. 1941. Rip currents: A process of geological importance. *Journal of Geology* 49 (4): 337–369.

Shepard, F.P., and D.L. Inman. 1950. Nearshore circulation related to bottom topography and wave refraction. *Transactions American Geophysical Union* 31: 196–212.

Short, A.D. 1985. Rip-current type, spacing and persistence, Narrabeen Beach, Australia. *Marine Geology* 65: 47–71.

Short, A.D., and C.L. Hogan. 1994. Rip currents and beach hazards: Their ımpact on public safety and ımplications for coastal management. *Journal of Coastal Research* 12: 197–209.

Shu, Y. 2015. *Future changes of the north West Pacific typhoons: Using the High resolution GCM EC-earth*, 1–22. Wageningen University Department of R&D Weather and Climate Modeling, Koninklijk: KNMI.

Ślączka, A., F. Nigro, P. Renda, and R. Favar. 2011. Lower Pleistocene deposits in east part of the Favignana Island, Sicily, Italy. *Italian Journal of Quaternary Sciences* 24 (2): 153–169.

Smith, J.A., and J.L. Largier. 1995. Observations of nearshore circulation: Rip currents. *Journal of Geophysical Research* 100: 10967–10975.

Sobel, A.H., S.J. Camargo, T.M. Hall, C.Y. Lee, M.K. Tippett, and A.A. Wing. 2016. Human influence on tropical cyclone intensity. *Science* 353 (6296): 242–246.

Spath, L.F. 1933. *Revision of Jurassic collection of ammonites of Kutch (cutch), pal*. India: Geological Society of India, New Sr. 9, Mem. 2.

Sugi, M., A. Noda, and N. Sato. 2002. Influence of the global warming on tropical cyclone climatology: An experiment with the JMA global model. *Journal of the Meteorological Society of Japan* 80 (2): 249–272.

Tam, G.K.W. 1973. Dynamics of rip currents. *Journal of Geophysical Research* 78: 1937–1943.

Terwindt, J.H.J. 1981. Origin and sequences of sedimentary structures in inshore mesotidal deposits of the North Sea. *Special Publication international Association of Sedimentologist* 5: 4–26.

Thompson, R.E. 1981. Oceanography of the British Columbia coast. *Canadian Special Publication of Fisheries and Aquatic Sciences* 50: 1–291.

Thornton, E.B., J. MacMahan, and A.H. Sallenger. 2007. Rip currents, mega-cusps, and eroding dunes. *Marine Geology* 240: 151–167.

Vail, P.R., R.M. Mitchum Jr., and S. Thompson. 1977. *Seismic stratigraphy and global changes of sea level, part 4: Global cycles of relative changes of sea level.*

Vos, R.G., and D.K. Hobday. 1977. Storm beach deposits in the late Paleozoic Ecca Group of South Africa. *Sedimentary Geology* 19: 217–232.

Wright, L.D. 1982. Field observations of long period surf zone oscillations in relation to contrasting beach morphologies. *Australian Journal of Marine and Freshwater Research* 33 (2): 181–201.

Wu, C.S., and P.L.F. Liu. 1985. Finite element analysis of nonlinear nearshore currents. *Journal of Waterway, Port, Coastal and Ocean Division, American Society of Civil Engineers* 111 (2): 417–432.

Yang, D.Y. 2010. Historical natural disasters and measures against them in Korea. *Trends Science* 15: 36–43.

Yang, D.Y., M. Han, J.C. Kim, Y.K. Cho, J.Y. Kim, S. Yi, K. Katsuki, and H.F.L. Williams. 2017. Shell and gravel layers caused by storm-induced rip currents during the medieval warm period and little ice age in South Korea. *Palaeogeography, Palaeoclimatology, Palaeoecologhy* 487: 204–215.

Publisher's Note